ASSESSMENT OF TWO DC VOLTAGE DROOP OPTIONS FOR SMALL-SIGNAL STABILITY IN MMC-BASED MULTI-TERMINAL DC GRIDS

Mohamed Elsodany[12] , Kosei Shinoda[1], Jing Dai[134], Alberto Bertinato[1], Seddik Bacha[12]*

[1]*Supergrid Institute SAS, 23 rue de Cyprian, 69100 Villeurbanne, France*
[2]*University Grenoble Alpes, CNRS, Grenoble INP, G2Elab, 38000 Grenoble, France*
[3]*Université Paris-Saclay, CentraleSupélec, CNRS, Laboratoire de Génie Electrique et Electronique de Paris, 91192, Gif-sur-Yvette, France.*
[4]*Sorbonne Université, CNRS, Laboratoire de Génie Electrique et Electronique de Paris, 75252, Paris, France*
**E-mail: mohamed.elsodany@supergrid-institute.com*

Keywords: MULIT-TERMINAL DC GRID, INTEROPERABILITY, DC VOLTAGE CONTROL, MODULAR MULTILEVEL CONVERTERS

Abstract

The paper studies the stability issue in a multi-terminal HVDC grid where multiple vendors implement different control strategies for DC voltage regulation. Small-signal analysis reveals the effects of the droop gain values of two control options, with one showing better robustness than the other. The effects of the response time of the outer control loops as well as those of the DC reactors are also investigated. The results of the small-signal analysis are supported by EMT simulations.

1 Introduction

Multi-terminal DC (MTDC) grids have garnered significant attention over the past decade as an efficient means of transferring a large amount of electricity from offshore wind farms. In comparison with point-to-point links, MTDCs offer superior reliability, efficiency and controllability [1, 2]. The planned MTDC projects will start with few connections and are expected to expand in terms of both the number of connections and the meshing level as the power capacity increases. In this context, multi-vendor grids comprising converter stations with plug-and-play capability are required [3], where the stability challenges have been identified [4–6]. In particular, it is probable that each vendor will implement the internal converter control without sharing all the information due to Intellectual Property (IP) concerns. However, the smooth harmonization between each vendor's specific control is key for a stable and reliable operation of DC grids.

Similar to frequency in AC systems, the DC voltage is the main indicator for power balance in DC systems. In addition, the DC voltage control is also organized in a hierarchical structure with primary, secondary and tertiary control layers [6, 7]. The methods at the primary level are categorized into master-slave control, voltage-margin control and droop control [7]. With the increasing expected number of terminals, DC voltage droop control is likely to be the preferred control strategy. By applying a proportional action on the DC voltage deviation, all droop-controlled stations participate in the DC voltage regulation after a power mismatch. Consequently , DC voltage droop control offers more reliability and redundancy compared to the well-known master-slave control which is more common in point-to-point links. Thus, the DC voltage droop control has been extensively studied in the literature [8–10].

The choice of the droop gain has been a subject of extensive research, which can be divided into two main classes: fixed droop gain and adaptive droop gain [8]. Fixed droop methods rely on assigning a constant droop gain to converter stations, regardless of their operating conditions and available reserves. However, this method is deemed unreliable, especially when converters need to operate at or near their rated conditions to achieve a higher capacity factor. Unlike synchronous generators in AC systems, where the Transmission System Operators (TSOs) mandate a sufficient reserve to ensure effective participation in frequency regulation [11], MTDC systems are typically considered as investments and converter stations are likely to operate close to their rated conditions. Hence, ensuring a flexible reserve to support the DC voltage regulation poses a significant challenge, particularly given the initially small number of planned connected stations for MTDCs. On the other hand, adaptive droop methods determine the droop gain based on various constraints, such as the proximity to converter limits and the strength of the connected AC system [8, 12, 13]. Nevertheless, these methods primarily address static considerations related to the droop gain, specifically its impact on steady-state power contributions in response to DC voltage mismatches.

One aspect that has received relatively less attention is the dynamic implications of the droop gain. In AC systems, the selection of the droop gain for frequency regulation primarily focuses on static considerations. This is because synchronous generators typically exhibit slow response times, making the stability implications of the droop gain less concerning. However, in a DC grid, rapid power responses can potentially

https://doi.org/10.1049/icp.2024.2199

lead to an excessive DC voltage deviation with more severe transients. Consequently, understanding and optimizing the dynamic effects of the droop gain in a DC system become crucial for ensuring overall system stability. In addition to the droop gain, the system stability also depends on other control parameters, such as the tuned response time of the inner power and voltage loops.

In a multi-vendor MTDC system, the implementation of the internal converter control and primary control is under the vendor's responsibility. Different realizations of the DC voltage droop control have been identified in [14]. In [15], stability assessment of some implementation options was carried out. Moreover, the interactions between different droop control strategies is a major interoperability issue. In [16], the interaction between different droop implementations was studied with a focus on VSC-based MTDCs. The results show that active power transfer capability is affected by the different combinations of droop control implementations.

The aim of this study is to assess the stability of Modular Multilevel Converter (MMC)-based MTDC system encompassing two different droop control implementations. The MMC is considered since it is the preferred converter topology for future MTDC expansion plans thanks to its modularity, efficiency and reliability. We will identify the implications of the droop gains when different control implementations coexist in an MTDC. The effect of the tuned response time of the inner control loops is also investigated. In addition, since one important protection element for future MTDCs is the DC breakers equipped with large DC inductors to limit fault currents [17], we also investigate the effects of large DC inductors connected at the terminals of converter stations on the dynamic performance and stability of the DC system. The main contributions of this study are:

- Identify the main oscillatory modes of an MMC-based MTDC system by means of a comprehensive small-signal analysis.
- Investigate the implications of the droop gain values, considering two droop implementation options present in a single DC system.
- Study the effect of the DC reactor size on the dynamic performance and stability of the MTDC, taking into account the two droop control options.

2 System modeling

The MMC model retained throughout this study is the Arm-Average Model (AAM) [18, 19] shown in Fig. 1, where the internal dynamics of the MMC are represented by 6 capacitors of size C_{eq}, one for each arm and in series with an inductance L_{arm} and a resistance R_{arm}. The AC terminals of the MMC are interfaced with the AC grid by an equivalent RL circuit denoted by R_{tr} and L_{tr}, respectively.

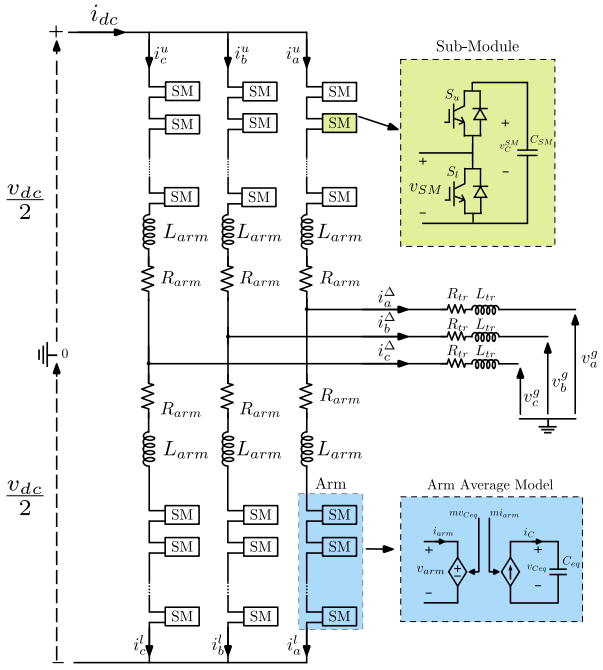

Fig. 1: Topology of a Modular Multilevel Converter.

Applying Kirchhoff's voltage law to phase $k \in \{a, b, c\}$, the following equations are deduced:

$$\begin{aligned} \frac{v_{dc}}{2} - v_k^u - L_{arm}\frac{di_k^u}{dt} - R_{arm}i_k^u - L_{tr}\frac{di_k^\Delta}{dt} - R_{tr}i_k^\Delta = v_k^g \\ -\frac{v_{dc}}{2} + v_k^l + L_{arm}\frac{di_k^l}{dt} + R_{arm}i_k^l - L_{tr}\frac{di_k^\Delta}{dt} - R_{tr}i_k^\Delta = v_k^g \end{aligned} \tag{1}$$

with $i_k^\Delta = i_k^u - i_k^l$.

By introducing the following variables with superscripts Σ and Δ, as in [20],

$$i_k^\Sigma = (i_k^u + i_k^l)/2, \quad v_k^\Delta = (-v_k^u + v_k^l)/2, \quad v_k^\Sigma = (v_k^u + v_k^l)/2 \tag{2}$$

equation (1) can be rewritten as:

$$\begin{aligned} L_{ac}\frac{di_k^\Delta}{dt} &= v_k^\Delta - v_k^g - R_{ac}i_k^\Delta \\ L_{arm}\frac{di_k^\Sigma}{dt} &= \frac{v_{dc}}{2} - v_k^\Sigma - R_{arm}i_k^\Sigma \end{aligned} \tag{3}$$

where $L_{ac} = L_{tr} + L_{arm}/2$ and $R_{ac} = R_{tr} + R_{arm}/2$ represent the equivalent AC-side inductance and resistance, respectively.

The equivalent arm capacitors are charged or discharged depending on the current direction. Formally, we have

$$C_{eq}\frac{dv_{Ck}^{u,l}}{dt} = i_{Ck}^{u,l} \tag{4}$$

The inserted voltages $v_k^{u,l}$ are calculated from the modulations indices and the equivalent capacitor voltages as $v_k^{u,l} = m_k^{u,l}v_c^{u,l}$. Similarly, the inserted currents $i_{Ck}^{u,l}$ charging the arm capacitors are calculated as $i_{Ck}^{u,l} = m_k^{u,l}i_k^{u,l}$.

By introducing the following notations

$$v_{Ck}^{\Delta} = (v_{Ck}^{u} - v_{Ck}^{l})/2, \qquad v_{Ck}^{\Sigma} = (v_{Ck}^{u} + v_{Ck}^{l})/2$$
$$m_{k}^{\Delta} = m_{k}^{u} - m_{k}^{l}, \qquad m_{k}^{\Sigma} = m_{k}^{u} + m_{k}^{l} \tag{5}$$

Equation (4) can be rewritten as:

$$2C_{eq}\frac{dv_{Ck}^{\Delta}}{dt} = m_{k}^{\Sigma}\frac{i_{k}^{\Delta}}{2} + m_{k}^{\Delta}i_{k}^{\Sigma}$$
$$2C_{eq}\frac{dv_{Ck}^{\Sigma}}{dt} = m_{k}^{\Delta}\frac{i_{k}^{\Delta}}{2} + m_{k}^{\Sigma}i_{k}^{\Sigma} \tag{6}$$

The park transformation is then applied to Eqs. (3) and (6) to obtain a time-invariant representation of the system [20], which is then linearized for the small-signal analysis.

3 MMC control

3.1 Inner control

The control of the MMC is depicted in Fig. 2. The inner control regulates the arm currents by generating the references for the modulation indices. The AC current control of the MMC is identical to that of a 2-level VSC, which is based on decoupling the dq components of the current and using a PI controller to follow the current references.

$$v_{d}^{\Delta *} = k_{p}^{i^{\Delta}}(i_{d}^{\Delta *} - i_{d}^{\Delta}) + \epsilon_{i_{d}^{\Delta}} + v_{d}^{g} - \omega L_{ac} i_{q}^{\Delta}$$
$$v_{q}^{\Delta *} = k_{p}^{i^{\Delta}}(i_{q}^{\Delta *} - i_{q}^{\Delta}) + \epsilon_{i_{q}^{\Delta}} + v_{q}^{g} + \omega L_{ac} i_{d}^{\Delta}$$

where $\epsilon_{i_{d}^{\Delta}}$ and $\epsilon_{i_{q}^{\Delta}}$ are the corresponding integral states of the dq current controllers.

$$\frac{d\epsilon_{i_{d}^{\Delta}}}{dt} = k_{i}^{i^{\Delta}}(i_{d}^{\Delta *} - i_{d}^{\Delta}) \tag{7}$$
$$\frac{d\epsilon_{i_{q}^{\Delta}}}{dt} = k_{i}^{i^{\Delta}}(i_{q}^{\Delta *} - i_{q}^{\Delta}) \tag{8}$$

The PLL dynamics are assumed ideal in this study, hence the perfect decoupling between the dq-axis quantities. In this study, the *Non-Energy-Based Control* is adopted [21], where the the internal energy of the MMC is not explicitly controlled. Instead, a pair of PI controllers are used to suppress the negative-sequence double-frequency harmonics, as shown in Fig. 2. The output of the i^{Δ} and i^{Σ} controllers are used to generate the inserted voltage references $v_{dq}^{\Delta *}$ and $v_{dq}^{\Sigma *}$, which in turn are divided by the DC voltage to generate the corresponding modulation indices by means of *direct modulation* [22].

3.2 Outer control

The outer control is responsible for regulating the DC voltage, and it generates the current references for the inner control loops accordingly. In this layer, two possible droop control options are considered, as depicted in Fig. 2. In scheme A, the droop gain is acting on the DC voltage control error to generate the AC power reference, and the AC power is controlled in closed loop by a PI control that generates the d-axis current reference. In scheme B, the droop gain acts on the AC power control error to generate a DC voltage reference, which is to be realized by a PI controller. To represent the integrator dynamics, an additional state equation is added to the state-space model:

$$\frac{d\epsilon_{P}}{dt} = k_{i}^{P}\left(\frac{-1}{k_{\text{droop}}}(v_{dc}^{\text{set}} - v_{dc}) + P_{ac}^{\text{set}} - P_{ac}\right) \tag{9}$$

if scheme A is used; or

$$\frac{d\epsilon_{v_{dc}}}{dt} = k_{i}^{v_{dc}}(-k_{\text{droop}}(P_{ac}^{\text{set}} - P_{ac}) + v_{dc}^{\text{set}} - v_{dc}) \tag{10}$$

if scheme B is used.

Based on (9) and (10), the reference for the d-axis current can be calculated:

$$i_{d}^{\Delta *} = \epsilon_{P} + k_{p}^{P}\left(\frac{-1}{k_{\text{droop}}}(v_{dc}^{\text{set}} - v_{dc}) + P_{ac}^{\text{set}} - P_{ac}\right) \tag{11}$$

if scheme A is used; or

$$i_{d}^{\Delta *} = \epsilon_{v_{dc}} + k_{p}^{v_{dc}}(-k_{\text{droop}}(P_{ac}^{\text{set}} - P_{ac}) + v_{dc}^{\text{set}} - v_{dc}) \tag{12}$$

if scheme B is used.

In [23], the two control options showed the same steady-state response. Thus, the aim of this study is to investigate the dynamic implications of the two controls.

The reference for the q-axis current $i_{q}^{\Delta *}$ is normally generated by a reactive power loop or an AC voltage control loop. Since the reactive power is not the focus of this paper, $i_{q}^{\Delta *}$ will be kept zero here.

4 MTDC system description

The three-terminal DC grid in asymmetrical monopole configuration shown in Fig. 3 is used to conduct the analysis, where Station 1 uses Scheme A while Station 2 uses Scheme B. The third terminal is connected to an ideal power source in parallel with a capacitor C_3, which serves as a simplified representation of a station operating in constant power mode. The key parameters of the system are given in Table 1. For ease of analysis, a lumped DC capacitor is used to represent the DC cables. The DC-voltage dynamics are represented by:

$$C_{dc}\frac{dv_{dc}}{dt} = \frac{P_{ext}}{v_{dc}} - i_{dc1} - i_{dc2} \tag{13}$$

where i_{dc1} and i_{dc2} are defined as in Fig. 3.

The closed-loop MIMO system in Fig. 3 is obtained by interconnecting and linearizing the respective subsystems. In order to validate the linearized model, a comparison with the original non-linear system simulated in EMTP-RV is conducted. A step change in the power injection of station 3 P_{ext} is introduced at $t = 3.5$ s. As shown in Fig. 4, the linearized model captures the dynamics of the EMT system and is thus validated for further small-signal analysis.

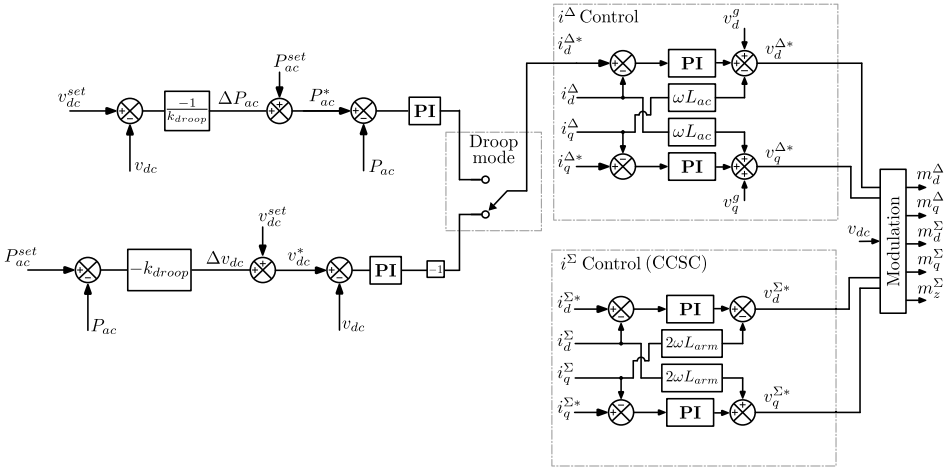

Fig. 2: MMC Control architecture.

Table 1 System parameters.

P_{nom}	1000 MW	v_{dc}^{nom}	640 kV
v_{ac}^{nom}	400kV RMS L − L	C_{arm}	32.55 μF
R_{arm}	80 mΩ	R_{tr}	0.512 Ω
L_{tr}	58.7 mH	C_0	1 μF
L_{arm}	48.9 mH	C_{dc}	20 μF
τ^P	50 ms	$\tau^{v_{dc}}$	50 ms

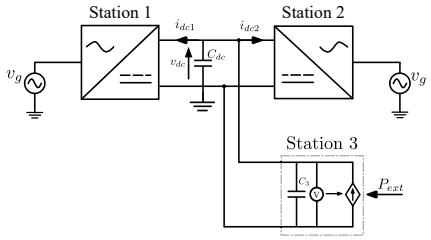

Fig. 3: 3-terminal HVDC system under study.

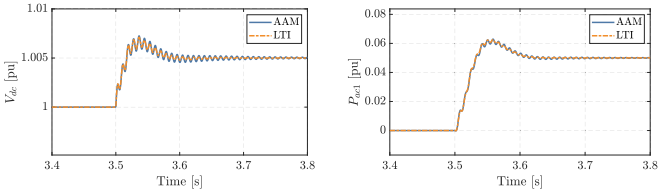

(a) DC Voltage

(b) AC Power of station 1

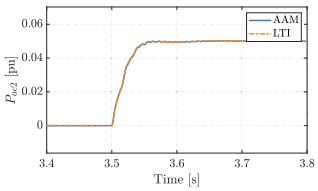

(c) AC Power of Station 2

Fig. 4: Validation of the linearized system.

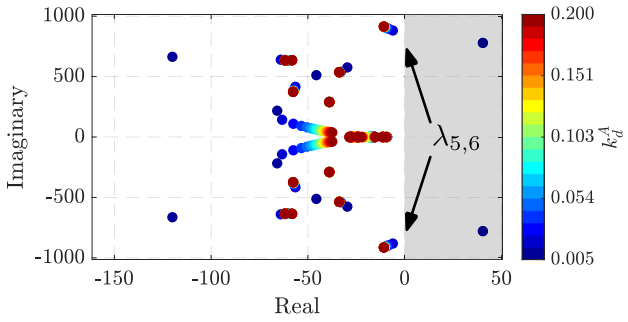

Fig. 5: Eigenvalues trajectories with different values of k_d^A while $k_d^B = 0.1$ pu.

5 Small-signal analysis

5.1 Effect of the droop gain

This subsection highlights the stability implications of the droop gain, especially when different implementation options are considered.

Fig. 5 shows the eigenvalues trajectories with different values of k_d^A of Station 1, while k_d^B of Station 2 is kept constant at 0.1 pu. It can be seen that, as k_d^A decreases, the pair of dominant poles migrate to the Right Half Plane (RHP) inferring system instability when $k_d^A = 0.005$ pu. This can be explained by considering the droop control loop shown in Fig. 2. In fact, a low value of k_d^A amplifies the gains of the power control loop for the same variation of the DC voltage, hence increasing the closed-loop bandwidth of the power loop. This may seem beneficial since the system reaches the steady state faster. However, a larger closed-loop bandwidth of the power loop also implies more undesirable interactions with the inner current loop. Thus, a decreasing k_d^A would eventually destabilize the system.

To see the participation level of the different states in the dominant poles $\lambda_{5,6}$, the results of a participation factor

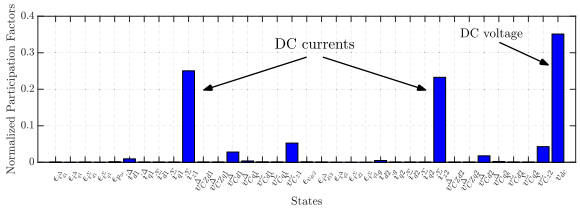

Fig. 6: Participation factor analysis of $\lambda_{5,6}$.

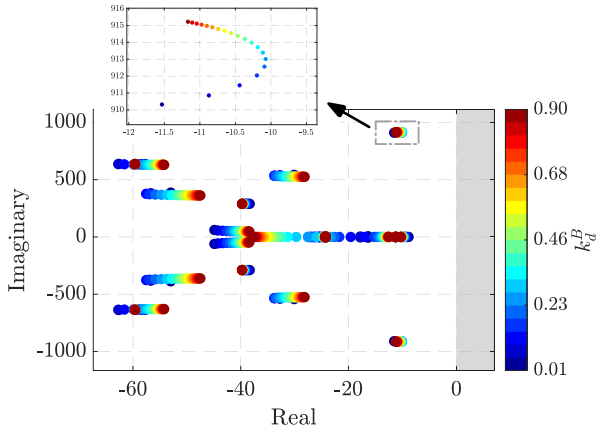

Fig. 7: Eigenvalues trajectories with different values of k_d^B while $k_d^A = 0.1$ pu.

analysis are shown in Fig. 6, where $\lambda_{5,6}$ are linked to the DC voltage and the DC currents.

The eigenvalues trajectories when changing k_d^B while $k_d^A = 0.1$ pu is shown in Fig. 7, which indicates a stable system for the whole considered range of k_d^B, i.e. $0.01 \leq k_d^B \leq 0.9$. It is worthnoting that system remains stable at both low and high droop gain values, with the intermediate range posing the sole potential risk of instability.

5.2 Effect of the response time of the outer control loops

This subsection investigates the stability implications of the tuned closed-loop response time of power τ_r^P for station 1 and the tuned closed-loop response time of DC voltage $\tau_r^{V_{dc}}$ for station 2. The results with a variation of k_d^A under two values of τ_r^P is given in Fig. 8, which show that, as the power-loop bandwidth decreases, i.e. with a higher value of τ_r^P, the minimum stable value of k_d^A decreases. In particular, choosing $k_d^A = 0.005$ pu used to result in instability with $\tau_r^P = 50$ ms, but no longer poses any stability risk when τ_r^P is increased to 100 ms. However, this comes at the cost of an overall slower power response.

Similarly, we change k_d^B for different values of $\tau_r^{V_{dc}}$. The result in Fig. 9 shows that, as $\tau_r^{V_{dc}}$ increases, $\lambda_{5,6}$ move further to the left of s plane, thus reducing the risk of instability. This result is in line with the intuition that, when the outer DC voltage loop has a slower response, its interaction with the inner current control is minimized. Moreover, as $\tau_r^{V_{dc}}$ increases, the impact of varying k_d^B becomes marginal, as the eigenvalues moves little when k_d^B changes.

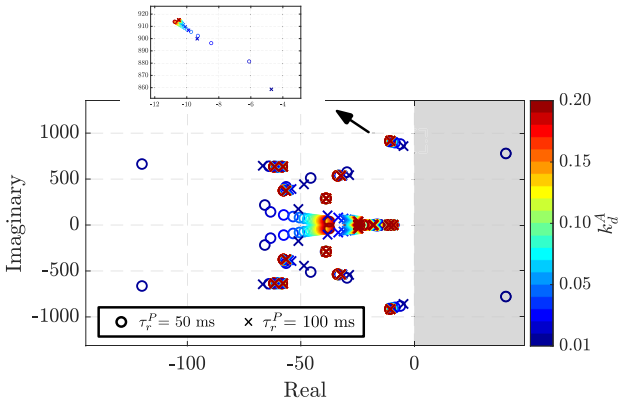

Fig. 8: Eigenvalue trajectories for the variation of k_d^A considering different values of τ_r^P.

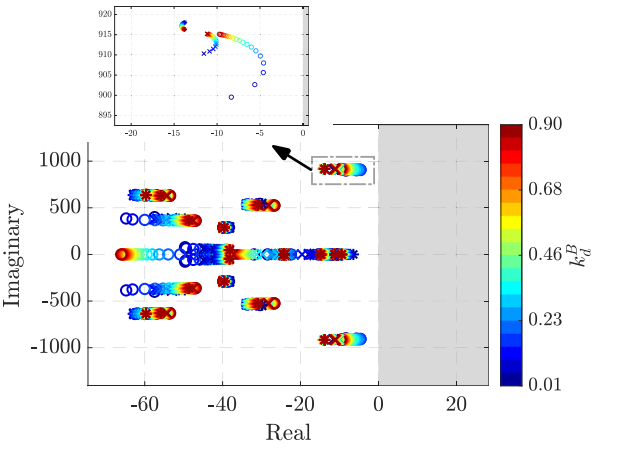

Fig. 9: Eigenvalue trajectories for the variation of k_d^B considering different values of $\tau_r^{V_{dc}}$.

6 Effects of DC reactors

In this section, the effects of the size of the DC inductance on the system stability are investigated. Furthermore, we explore the relationship between the feasible values of droop gains and the potential limitations imposed by the DC reactors.

Fig. 10 depicts the modified MTDC system where two inductors of values L_{DCCB} are introduced to represent the DCR. A small capacitance is added to the terminals of stations 1 and 2 to distinguish their respective DC voltages. Thus, four additional state variables are added to the small-signal model, namely I_{DCCB1}, I_{DCCB2}, v_{dc1} and v_{dc2}, while the previously defined DC voltage v_{dc} corresponds now to the voltage at the terminals of station 3 v_{dc3}, whose connection to C_{dc} has no DC breaker.

Fig. 11 shows the Bode magnitude diagram of the transfer function $\Delta v_{dc3}/\Delta P_{ext}$ for three values of DCR size, with

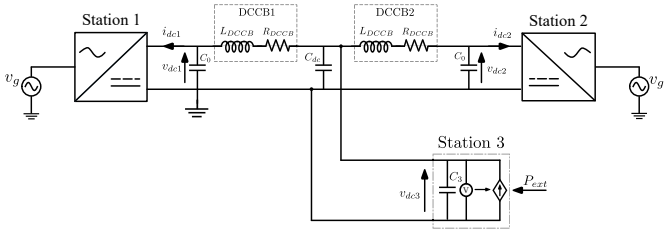

Fig. 10: 3-terminal HVDC system with DCCB.

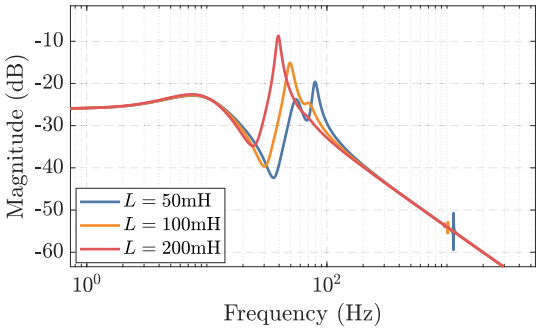

Fig. 11: Bode diagram of the transfer function $\frac{\Delta v_{dc3}}{\Delta P_3}$ for different values of L_{DCCB}.

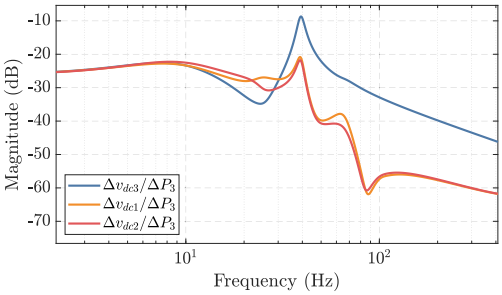

Fig. 12: Bode diagram of the transfer function from v_{dc1}, v_{dc2} and v_{dc3} to P_3, with $L_{\text{DCCB}} = 200$ mH.

$k_d^A = k_d^B = 0.1$ pu. A higher resonant peak is observed as L_{DCCB} increases. The resulting higher resonant peaks indicate a deteriorated damping at the corresponding frequency. The Bode diagram of the DC voltages of the three stations to a power disturbance from station 3 is shown in Fig. 12, where the highest resonant peak is observed at v_{dc3} compared to v_{dc1} and v_{dc2}. In fact, a higher inductance value increases the electrical distance between the stations, which delays the response of the DC voltage control loop of Stations 1 and 2 to the power disturbance from Station 3, making v_{dc3} more susceptible to deteriorated damping. This confirms the results of [24], which pointed out the necessity of a sufficient number of DC voltage droop-controlling stations in an MTDC to damp the DC voltage oscillations.

The effect of the DCR size considering different values of k_d^A and k_d^B is shown in Fig. 13, which gives the maximum magnitude of the frequency response of the transfer function

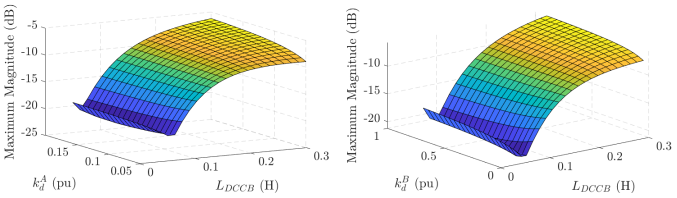

(a) (b)

Fig. 13: Maximum resonant peak of the frequency response of the transfer function $\Delta v_{dc3}/\Delta P_3$ with different values of k_d^A, k_d^B and the DCR size.

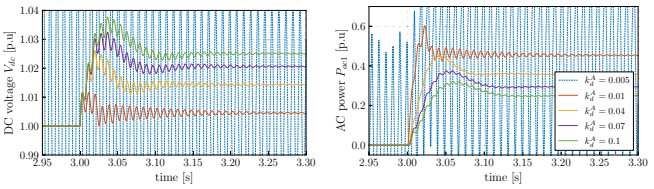

(a) DC Voltage (b) AC Power of station 1

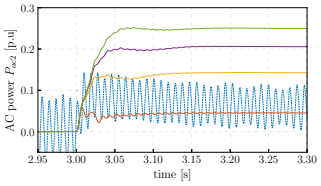

(c) AC Power of Station 2

Fig. 14: Simulation results on the effect of varying k_d^A.

$\Delta v_{dc3}/\Delta P_{ext}$. Note that both k_d^A and k_d^B only slightly impacts the trend observed in Fig. 11.

7 Simulation results

In this section, the conclusions of the above small-signal analysis are verified by time-domain simulations on the EMT model implemented in EMTP-RV in Fig. 3, where the MTDC is connected in an asymmetrical monopole configuration.

The original operating point corresponds to no power flow in the MTDC. In the first scenario, a 0.5 pu step increase in the power reference of Station 3 is introduced at $t = 3$ s. Different values of k_d^A are tested with $k_d^B = 0.1$ pu. The results in Fig. 14 shows a clear trend: the system's damping degrades as k_d^A decreases. At $k_d^A = 0.005$ pu, the system becomes unstable. This observation is in line with the findings of the small-signal analysis, which indicated the lower limit of $k_d^A = 0.005$ pu that could lead to instability. Note that the PI controllers implemented in the EMT model are equipped with anti-wind scheme that limit the controller output. However, the persisting oscillations infer instability at $k_d^A = 0.005$ even if the oscillation are not growing in magnitude.

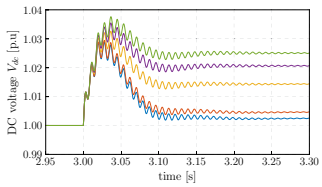

(a) DC Voltage

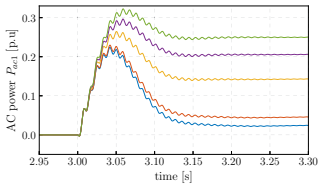

(b) AC Power of station 1

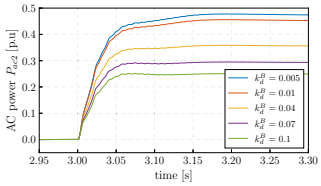

(c) AC Power of Station 2

Fig. 15: Simulation results on the effect of varying k_d^B.

In the second scenario, k_d^B is varied, with $k_d^A = 0.1$ pu. The results in Fig. 15 shows that the system remains stable for the entire considered range of k_d^B, as predicted by the small-signal analysis. This stability is maintained even at low values of droop gain ($k_d^B = 0.005$ pu), an unstable value for k_d^A of Station 1. This shows the better robustness of scheme B compared to scheme A.

To test the effect of the DCR size on the transient response of the system. The setup depicted in Fig. 10 is considered. A 0.5 pu power reference increase in station 3 is introduced at $t = 3$ s. Fig. 16 shows the DC voltage measured at the terminals of station 3 for different combinations of droop gains and DC reactor values. The global trend shows a deteriorated damping in the transient as the DCR size increases. However, the system remains stable even after the abrupt transients. This trend is observed for different values of k_d^A and k_d^B, as already shown by the small-signal analysis in Fig. 13.

8 Conclusions

This study of small-signal stability of an MTDC grid investigated two droop control options: Schemes A and B. We revealed that Scheme B outperforms Scheme A in maintaining system stability at lower droop gain values, supported by small-signal analysis and time-domain simulations. The tuning of PI controllers in the power loop of Scheme A and the DC voltage loop in Scheme B was identified as a crucial factor affecting the feasible range of droop gains. Additionally, a larger DC reactor size could negatively affect the transient response of the system, especially for the DC voltages measured at the terminals of power controlling stations. In the future, dedicated controllers to damp the oscillatory modes should be considered to ensure a robust MTDC system operation.

9 Acknowledgements

This work was supported by InterOPERA project under the grant agreement No. 101095874. Views expressed are however those of the authors only and do not necessarily reflect those of the European Union or CINEA. Neither the European Union nor the granting authority can be held responsible for them.

10 References

[1] J. A. Ansari, C. Liu, and S. A. Khan, "MMC Based MTDC Grids: A Detailed Review on Issues and Challenges for Operation, Control and Protection Schemes," *IEEE Access*, vol. 8, pp. 168 154–168 165, 2020.

[2] B. Luscan, S. Bacha, A. Benchaib, A. Bertinato, L. Chedot, J. C. Gonzalez-Torres, S. Poullain, M. Romero-Rodriguez, and K. Shinoda, "A vision of hvdc key role toward fault-tolerant and stable ac/dc grids," *IEEE Journal of Emerging and Selected Topics in Power Electronics*, vol. 9, no. 6, pp. 7471–7485, Dec. 2021.

[3] E.-E. T. Eurpope; Wind Europe, "Workstream for the development of multi-vendor HVDC systems and other power electronics interfaced devices," ENTSO-E, Tech. Rep., 2021.

[4] P. Rault, F. Colas, X. Guillaud, and S. Nguefeu, "Method for small signal stability analysis of VSC-MTDC grids," in *2012 IEEE Power and Energy Society General Meeting*. IEEE, jul 2012.

[5] N. R. Chaudhuri, R. Majumder, B. Chaudhuri, and J. Pan, "Stability Analysis of VSC MTDC Grids Connected to Multimachine AC Systems," *IEEE Transactions on Power Delivery*, vol. 26, no. 4, pp. 2774–2784, oct 2011.

[6] J. Beerten, S. Cole, and R. Belmans, "Modeling of Multi-Terminal VSC HVDC Systems With Distributed DC Voltage Control," *IEEE Transactions on Power Systems*, vol. 29, no. 1, pp. 34–42, jan 2014.

[7] D9.3, "Final Recommendations For Interoperability of Multivendor HVDC Systems," BEST PATHS, Tech. Rep., 2018.

[8] N. R. Chaudhuri and B. Chaudhuri, "Adaptive Droop Control for Effective Power Sharing in Multi-Terminal DC (MTDC) Grids," *IEEE Transactions on Power Systems*, vol. 28, no. 1, pp. 21–29, feb 2013.

[9] Y. Wang, F. Qiu, G. Liu, M. Lei, C. Yang, and C. Wang, "Adaptive Reference Power Based Voltage Droop Control for VSC-MTDC Systems," *Journal of Modern Power Systems and Clean Energy*, vol. 11, no. 1, pp. 381–388, 2023.

[10] K. Shinoda, A. Benchaib, J. Dai, and X. Guillaud, "Over- and Under-Voltage Containment Reserves for Droop-Based Primary Voltage Control of MTDC Grids," *IEEE Transactions on Power Delivery*, vol. 37, no. 1, pp. 125–135, feb 2022.

[11] ENTSO-E, "Network Code on Load-Frequency Control and Reserves," ENTSO-E, Tech. Rep., 2013.

[12] Y. Li, J. Zhao, H. Liu, Q. Kong, Y. Zhao, L. Cheng, and Z. Wang, "Adaptive Droop Control of the VSC-MTDC Distribution Network Considering Power & Voltage Deviation," *Frontiers in Energy Research*, vol. 9, feb 2022.

[13] J. Beerten and R. Belmans, "Analysis of Power Sharing and Voltage Deviations in Droop-Controlled DC Grids," *IEEE Transactions on Power Systems*, vol. 28, no. 4, pp. 4588–4597, nov 2013.

[14] F. Thams, S. Chatzivasileiadis, and R. Eriksson, "DC voltage droop control structures and its impact on the interaction modes in interconnected AC-HVDC systems," in *2017 IEEE Innovative Smart Grid Technologies - Asia (ISGT-Asia)*. IEEE, dec 2017.

[15] W. Wang, M. Barnes, and O. Marjanovic, "Stability limitation and analytical evaluation of voltage droop controllers for VSC MTDC," *CSEE Journal of Power and Energy Systems*, vol. 4, no. 2, pp. 238–249, jun 2018.

[16] F. Thams, R. Eriksson, and M. Molinas, "Interaction of Droop Control Structures and Its Inherent Effect on the Power Transfer Limits in Multiterminal VSC-HVDC," *IEEE Transactions on Power Delivery*, vol. 32, no. 1, pp. 182–192, feb 2017.

[17] M. Barnes, D. S. Vilchis-Rodriguez, X. Pei, R. Shuttleworth, O. Cwikowski, and A. C. Smith, "HVDC Circuit Breakers–A Review," *IEEE Access*, vol. 8, pp. 211 829–211 848, 2020.

[18] H. Saad, S. Dennetiere, J. Mahseredjian, P. Delarue, X. Guillaud, J. Peralta, and S. Nguefeu, "Modular Multilevel Converter Models for Electromagnetic Transients," *IEEE Transactions on Power Delivery*, vol. 29, no. 3, pp. 1481–1489, jun 2014.

[19] A. Zama, S. Bacha, A. Benchaib, D. Frey, and S. Silvant, "A novel modular multilevel converter modelling technique based on semi-analytical models for HVDC application," *Journal of Electrical Systems*, 2016.

[20] G. Bergna-Diaz, J. Freytes, X. Guillaud, S. D'Arco, and J. A. Suul, "Generalized Voltage-Based State-Space Modeling of Modular Multilevel Converters With Constant Equilibrium in Steady State," *IEEE Journal of Emerging and Selected Topics in Power Electronics*, vol. 6, no. 2, pp. 707–725, jun 2018.

[21] S. Samimi, "Modélisation et Commande des Convertisseurs MMC en vue de leur Intégration dans le Réseau Electrique," Ph.D. dissertation, CENTRALE LILLE, 2016.

[22] K. Sharifabadi, L. Harnefors, R. Teodorescu, S. Norrga, and H. P. Nee, *Design, Control, and Application of Modular Multilevel Converters for HVDC Transmission Systems*. Wiley Sons, Incorporated, John, 2016.

[23] K. Shinoda, M. Elsodany, J.-C. Gonzalez, J. Dai, A. Benchaib, and S. Bacha, "Comparison between DC Voltage Droop Schemes and Grid-Following & Grid-Forming Control in AC Systems in View of Interoperability of MTDC grids," in *2023 25th European Conference on Power Electronics and Applications (EPE'23 ECCE Europe)*. IEEE, sep 2023.

[24] W. Wang, M. Barnes, O. Marjanovic, and O. Cwikowski, "Impact of DC Breaker Systems on Multiterminal VSC-HVDC Stability," *IEEE Transactions on Power Delivery*, vol. 31, no. 2, pp. 769–779, apr 2016.

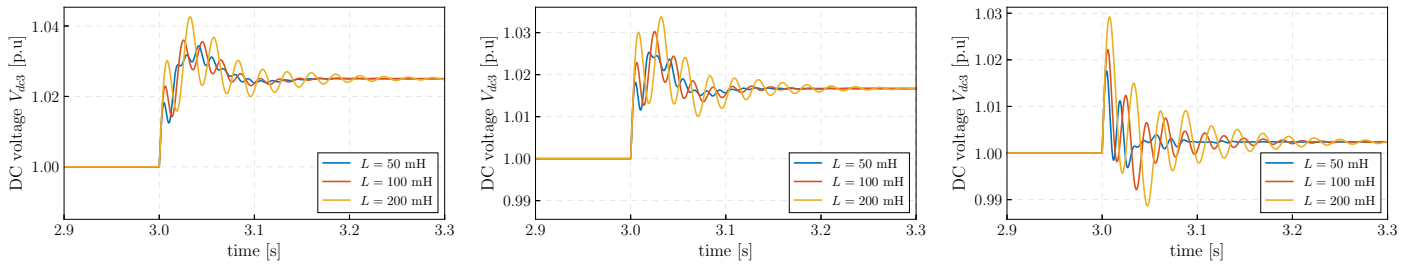

(a) $k_d^A = 0.1$ pu, $k_d^B = 0.1$ pu (b) $k_d^A = 0.05$ pu, $k_d^B = 0.1$ pu (c) $k_d^A = 0.005$ pu, $k_d^B = 0.1$ pu

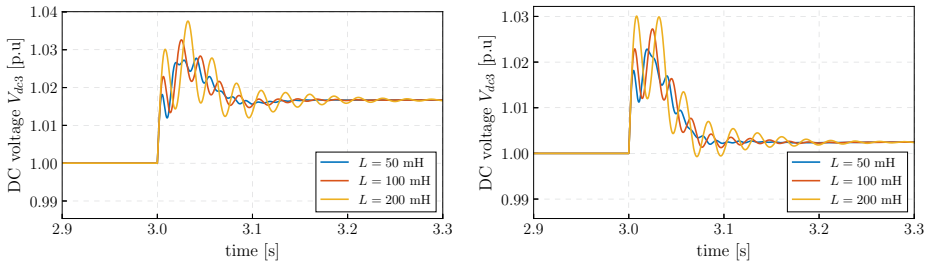

(d) $k_d^A = 0.1$ pu, $k_d^B = 0.05$ pu (e) $k_d^A = 0.1$ pu, $k_d^B = 0.005$ pu

Fig. 16: Simulation results on the effect of the DCR value on transient DC voltage response at station 3.